Simulation and Analysis of Walking on Compliant Surfaces

by

Junxin Wang

A Thesis Presented in Partial Fulfillment
of the Requirements for the Degree
Master of Science

Approved April 2019 by the
Graduate Supervisory Committee:

Panagiotis Artemiadis, Chair
Sze Zheng Yong
Hyunglae Lee

ARIZONA STATE UNIVERSITY

May 2019

ABSTRACT

There are a large group of amputees living in the country and the number of them is supposed to increase a lot in the following years. Among them, lower-limb amputees are the majority. In order to improve the locomotion of lower-limb amputees, many prostheses have been developed. Most commercially available prostheses are passive. They can not actively provide pure torque as an intact human could do. Powered prostheses have been the focus during the past decades. Some advanced prostheses have been successful in walking on level ground as well as on inclined surface and climbing stairs. However, not much work has been done regarding walking on compliant surfaces. My preliminary studies on myoelectric signals of the lower limbs during walking showed that there exists difference in muscle activation when walking on compliant surfaces. However, the mapping of muscle activities to joint torques for a prosthesis that will be capable of providing the required control to walk on compliant surfaces is not straightforward. In order to explore the effects of surface compliance on leg joint torque, a dynamic model of the lower limb was built using Simscape. The simulated walker (android) was commanded to track the same kinematics data of intact human walking on solid surface. Multiple simulations were done while varying ground stiffness in order to see how the torque at the leg joints would change as a function of the ground compliance. The results of this study could be used for the control of powered prostheses for robust walking on compliant surfaces.

ACKNOWLEDGMENTS

I would like to thank Dr. Artemiadis for being my first teacher in the United States and my research advisor. You have always been friendly and helpful.

I would like to thank Dr. Yong and Dr. Lee for their support and willingness to serve as my committee members.

I would also like to thank all the members of HORC lab for their kindness and help.

TABLE OF CONTENTS

CHAPTER Page

LIST OF TABLES

Table Page

LIST OF FIGURES

Figure Page

Chapter 1

INTRODUCTION

In the United States, there are about 2.2 million people who live with limb amputation, which corresponds to 0.68% of the total population. This number is expected to reach 3.6 million by the year 2050 (Ziegler-Graham *et al.* (2008)). Among them, most are lower-limb amputees. Amputation brings many inconvenience and discomfort to amputees. Besides the most commonly known phantom pain, amputees would also encounter difficulties in everyday activities such as locomotion. Lower-limb amputees usually spend more energy to walk than intact people (Schmalz *et al.* (2002)). Almost half of them have fear of falling and even experience falls (Miller *et al.* (2001)). Also, they often show an asymmetry in walking (Nolan *et al.* (2003)).

1.1 Prostheses

In order to improve the locomotion of lower-limb amputees, people have made a lot of efforts since centuries ago. It is said that a bronze-made artificial leg which is supposed to be date back to 300BC was unearthed in Italy according to an article posted on the website of Museum of Applied Arts and Sciences, Sydney, Australia. Nowadays, with the development of science and technology, many prostheses have been developed. The early prostheses are mainly passive and passive prostheses are still the most commonly used prostheses in the world. According to the 2018 annual report of Ossur, one of the largest non-invasive orthopaedics companies, powered prosthesis accounted for only 22 % of prosthetic component sales in 2018. Elastic parts such as spring are widely used on passive prostheses to store energy upon heel strike and then release to assist push off. Some researchers have been studying the

quasi-passive prostheses which can delay the release of energy until the designed toe-off time (Li *et al.* (2006)). However, they are still unable to actively provide torque as an intact ankle joint could do. Although people have thought of the concept of powered ankle prostheses since the 1990s, not many of them have brought the idea to life (Au *et al.* (2007)). In the past twenty years, the desire of improving the quality of life for lower-limb amputees has pushed the development of advanced prostheses. Many novel designs and control systems have been made. Some advanced prostheses have the ability to adapt to stairs and terrains of different inclination (Au *et al.* (2008)). However, few prostheses are designed for compliant surface walking.

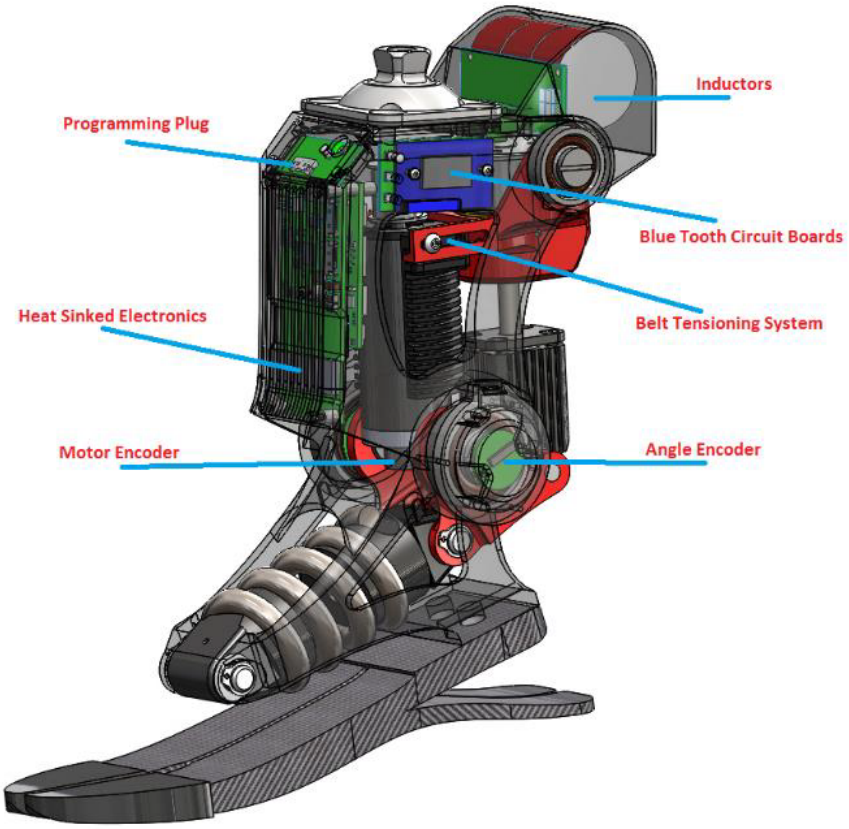

Figure 1.1: Odyssey Prosthesis by SpringActive Inc, Grimmer *et al.* (2016)

In order to build a smart ankle prosthesis that can adapt to compliant surfaces, Arizona State University is collaborating with SpringActive Inc. The prototype of

the ankle prosthesis is the Odyssey prosthesis developed by SpringActive Inc, shown in Fig. 1.1.

It has a compliant actuator to store energy gained at heel strike. A motor is embedded to provide energy actively. The Odyssey prosthesis has a rate gyro sensor combined with a two-axis accelerometer (Grimmer *et al.* (2016)). These sensors can give the information of angular velocity and acceleration which is used to determine the gait mode, speed, and progression percentage. Then the motor trajectory is generated according to these data. The experiment results showed that this ankle performs well in tasks of walking and running up to 2.6m/s on solid ground (Grimmer *et al.* (2016)).

1.2 Motivation - Myoelectric Differences Between Solid and Compliant Surfaces

In order to make the ankle prosthesis able to identify and adapt to the dynamic environment and requirements involved in a variety of real-life situations, we need to find out what happens to our muscles while walking on compliant surfaces. Several experiments were done to measure the muscles' activity when walking on compliant surfaces. Two different surfaces were used in the experiment. One is the normal solid ground while the other is a soft foam mat. Since the ankle prosthesis is supposed to move only in the sagittal plane, the main focus was on dorsiflexion and plantar flexion of the ankle joint. Three major muscles are considered to be dorsiflexors, which are tibialis anterior (TA), extensor hallucis longus and extensor digitorum longus. Among these three muscles, the tibialis anterior has the largest cross-section and is the easiest to locate. Previous research indicates that seven muscles serve as plantar flexors (Perry *et al.* (1992)). After several trials, I decided to use peroneus longus (PL) as the measurement for plantar flexion. The EMG data were measured using wireless EMG Sensors SP-W01D from Delsys. The sensor has an integrated

triaxial accelerometer and an EMG signal sampling rate of 2000 samples/sec. The raw EMG data was filtered using a moving window of root mean square (RMS) filter over every 500 samples. Experiments were done with an intact subject. 62 steps for rigid surface walking and 57 steps for soft surface walking were extracted and processed. The subject was walking at a constant speed of 90 steps per minute. All data was collected from the right leg. Figures 1.2 and 1.3 shows the experimental results. The solid line represents the mean of the corresponding EMG data while the shaded area represents the standard deviation. The horizontal axis is the normalized percent gait cycle with 0 representing heel strike. From the plot below we can find out some obvious differences.

The peroneus longus was activated more during stance phase while the TA re-

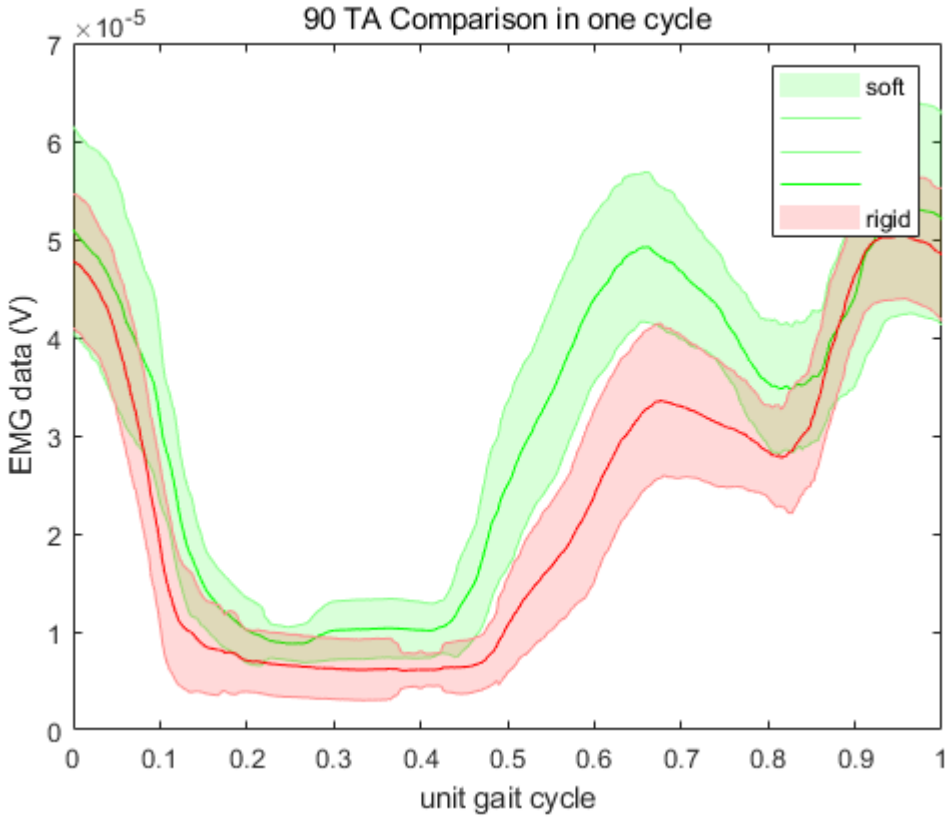

Figure 1.2: Comparison of TA Activation During the Gait Cycle Between Soft and Rigid Walking Surfaces.

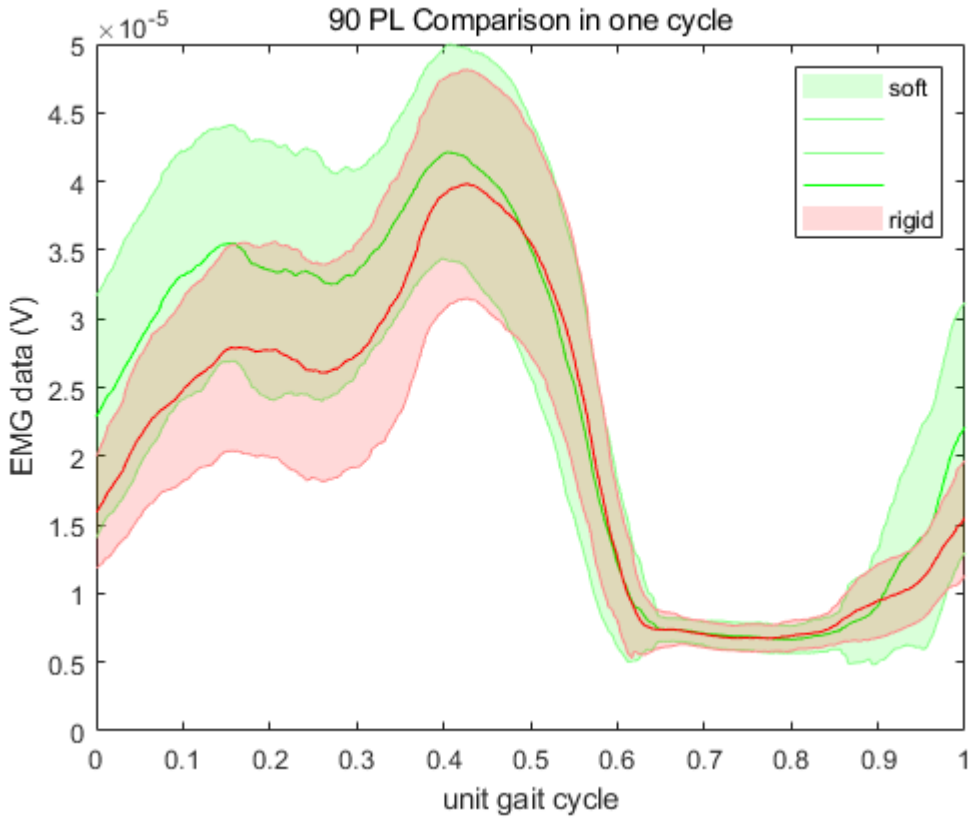

Figure 1.3: Comparison of PL Activation During the Gait Cycle Between Soft and Rigid Walking Surfaces.

mained almost the same on two surfaces. This corresponds with the results from the kinematics experiment, which is that the subject tends to flatten the foot as soon as possible upon stepping on a soft surface. The TA activation during early swing was larger on the soft surface while there was not much difference in PL activation. This might be because of the intention of increasing foot clearance to avoid trip-related falling as the foot sunk into the soft surface.

From the EMG experiments, we can see that there is an obvious difference in muscle activation while walking on compliant surfaces. Thus, we are expecting the ankle joint torque to be different on compliant surfaces too. However, the mapping of muscle activities to joint torques can be quite difficult for the lower limb. Also, with current equipment in the lab, it is not possible to measure the joint torques directly.

Therefore, we were considering to construct a dynamic model to simulate human walking on compliant surfaces. The results might be able to help the development of prosthesis control algorithm in the future.

Chapter 2

LITERATURE REVIEW

Previous research on modeling and simulation of human locomotion in order to help the design of biped robots and human gait research has been extensive. With the development of computational science and technology, many different methods have been put into use. In general, five physics-based methods are widely used. These are: the inverted pendulum model, passive dynamics walking method, zero moment point (ZMP) method, optimization-based method and control-based method (Xiang *et al.* (2010)).

2.1 Inverted Pendulum Model

Inverted pendulum model was first introduced as a control method for biped locomotion on rugged terrain (Kajita and Tani (1991)). By assuming an ideal robot model with massless legs and simplified movement, the legs can be treated as linear inverted pendulums. Constraints are applied to the original governing equations for the pendulum to get the desired performance of the robot. In this case, the inverted pendulum has only one point-mass at the end of the pendulum. In order to improve model accuracy and achieve more stable motions, researchers have tried to improved the complexity of the inverted pendulum model. For example, gravity-compensated inverted pendulum model was proposed by treating the free leg as an extra pendulum connected to the body (Park and Kim (1998)). A further developed version added more mass to the original model making it a multi-pendulum system (Albert and Gerth (2003)). Not only the complexity of the inverted pendulum model has increased, but also the application has been extended from 2-D to 3-D (Kajita

et al. (2001)).

2.2 Passive Dynamics Walking Method

Passive dynamics walking method, as its name indicates, originally aroused from biped robots with no actuators that can walk passively downhill under the effect of gravity. Take a simple compass model as an example. When it moves downhill, one leg stands on the ground as the stance leg while the other serves as the swing leg. The stance leg performs as an inverted pendulum and the swing leg as a normal pendulum. Under gravity, these legs swing and exchange the role with each other. The robot is thereby walking passively downhill. Researchers have been looking into such gait to study its dynamics and stability (McGeer *et al.* (1990)). By introducing actuators to the system, the passive walking can walk actively not only downhill but also on level ground (Collins *et al.* (2005)). Like inverted pendulum model, in the past decades, passive dynamics walking method also saw an increase in model complexity as researchers added more joints and other components to the original model to make it more human-like (Borzova and Hurmuzlu (2004)).

2.3 Zero Moment Point (ZMP)-Based Method

Zero moment point plays a vital role in balancing bipedal robots. It was first proposed half a century ago by Miomir Vukobratovic and Davor Juricic (Vukobratovic and Juricic (1969)). ZMP is defined as that point on the ground at which the net moment of the inertial forces and the gravity forces has no component along the horizontal axes (Vukobratović and Borovac (2004)). The ZMP-based method usually requires to generate a well-planned ZMP trajectory for the robot to follow. Furthermore, the full gait motion can be generated. But not all the planned ZMP trajectories can be feasible. Some researchers proposed a method where hip motion

is designed first and simulation and experiment result showed good stability (Huang *et al.* (2001)).

2.4 Optimization-Based Method

The optimization-based method uses numerical optimization techniques. The strategy is to minimize the cost function subjected to pre-defined constraints. For example, the physical limitation. This theory was stated to be able to help the research about walking on stairs or over holes (Chow and Jacobson (1971)). There are many choices of objective functions. Some researchers minimize mechanical energy (Chow and Jacobson (1971)), some maximize stability (Huang *et al.* (2001)) and so on.

2.5 Control-Based Method

The control-based method tries to simulate human walking by mimicking human control system (Xiang *et al.* (2010)). One way is to build controllers to track desired trajectories, such as joint angle trajectory. This is the method used in this research. Such trajectories can be obtained through experiment or from other methods such as ZMP method.

2.6 Conclusion

Although many different methods have been used to simulate human walking in the past, most of the previous research has focused on walking on solid ground. The environment is mainly level ground, stairs, and inclined surfaces. Not much work has been done on compliant surface walking.

Chapter 3

METHODOLOGY

3.1 Simscape Introduction (Simscape (2018))

A walking model was built in Simulink using Simscape. Simscape is provided by MathWorks, Inc as a set of block libraries and special simulation features for modeling physical systems in the Simulink environment. It was originally known as SimMechanics in its earlier version several years ago. According to its user guide, Simscape uses a different way of modeling compared to conventional Simulink model which is called the Physical Network approach. Every block in Simscape is a representation of basic mathematical operations. By connecting them together to create a physical model, the mathematical model is formed.

3.2 Physical Network Approach (Miller and MathWorks (2009))

The purpose of developing the Physical Network approach was to make the model of complex physical systems, especially those systems across multiple physical domains, reusable and easier to build. The inspiration for it came from electrical systems where Kirchhoff's laws are widely used. Kirchhoff's laws consist of two rules that deal with voltage and current. Kirchhoff's current law (KCL) says that the sum of currents flowing into a node equals the sum of currents flowing out of the same node. Kirchhoff's voltage law (KVL) states that, around any closed loop, the sum of voltages is zero. Also, notice that the product of current and voltage is power. The basic idea of Physical Network approach is the similarities between a common physical system and the electrical system. It uses variables in the physical system

that are analogous to current and voltage. For example, the voltage of a revolution joint is the angular velocity and the current is torque. Connecting two revolute joint together to build a simple model. In this system, KCL indicates that the torque flowing into the connection node equals the torque flowing out of this node while KVL indicates that the angular velocity of these two joints is the same. Variables that are analogous to voltage are referred to as across variables and those analogous to current are referred to as through variables in the Physical Network method. By using these variables, it is possible to apply KCL and KVL to the whole connected physical system to construct the mathematical relationship between all blocks. In this research, only two physical domains, mechanical rotational domain, and mechanical translational domain, are used. The across variables are angular velocity and translational velocity, respectively. The through variables are torque and force, respectively. Based on the physical network configuration, Simscape formulates the differential algebraic equations (DAE) for the model. Then it solves these equations using Simulink and Simscape solvers. In this research, ode45 was used. The flow chart of Simscape is shown in Fig. 3.1.

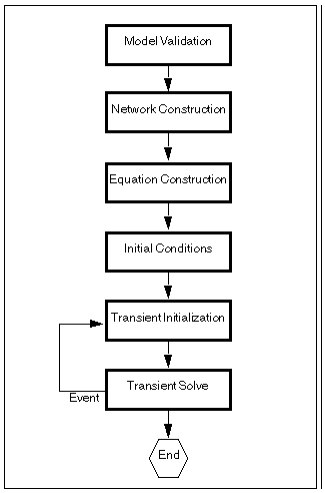

Figure 3.1: Simscape Flow Chart Showing How Simscape Simulation Works, Simscape (2018)

3.3 Model Setup

3.3.1 Android

A simplified human walking model (the Android) is discussed in this section. Since the main focus of the research is on the lower limb, the upper body and hip are replaced by a sphere with its center at the same height of hip joints. It has 6 revolute joints (hip, knee, ankle for each leg) which move only in the sagittal plane. That means this model does not have the ability to move in the frontal plane. Since the ankle prosthesis is also designed to move only in the sagittal plane, this simplification is currently acceptable.

The physical specifications of the model are given in the following table:

Table 3.1: Physical Specifications of the Android

Part	**Weight(kg)**	**Geometry**
Body	30	Sphere (Radius=0.2m)
Thigh	10	Cylinder (Radius=0.05m, height=0.4m)
Shank	5	Cylinder (Radius=0.05m, height=0.4m)
Foot	2	Cuboid (Length=0.23m, Width=0.1m, Hieght=0.05m)

The total weight of the android is 64kg. All joints are placed at the center of the top and bottom surfaces of the cylinder with a spring stiffness of 10 Nm/deg and damping coefficient of 1 Nm/(deg/s). Actually, the stiffness and damping coefficient of the joints are variables to muscle activity (Lee *et al.* (2016)). However, for simplicity, they are set as constant values in this model. The hip joints are placed on the horizontal axis of the sphere. There is a 0.05m offset applied to the ankle joint to move it backward in order to compensate for the toe joint. Because the actual human feet

have multiple joints (Larsen (2002)), especially the toe joints, the distance between the foot-ground contact point and heel would be smaller than total foot length.

The contact force between the android and the ground is simulated using sphere-to-plane contact. That is, the contact between the android and the ground is treated as a several-point contact. In this case, every foot cuboid has four contact points at each corner of the bottom surface (Frame 1 to 4 in Fig. 3.2). The coefficient of kinetic friction is set to 0.7 and the coefficient of static friction is set to 0.8. The velocity threshold between static and kinetic friction is 0.1m/s. These are consistent throughout the entire simulation.

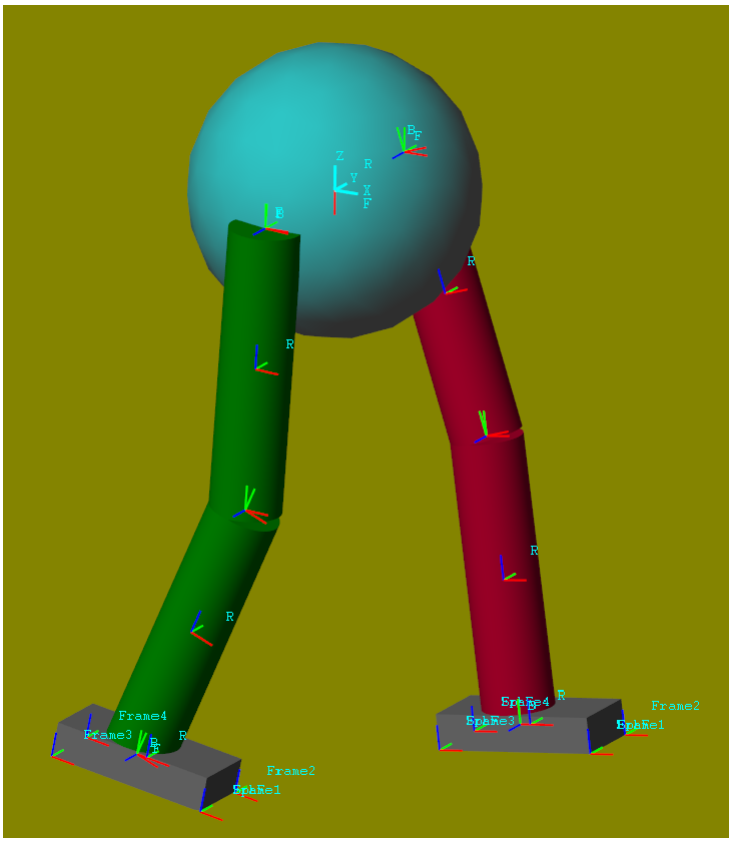

Figure 3.2: Android with Frames for Each Part and Contact Points.

3.3.2 *Ground*

The ground was modeled as a spring with a damper. The ground stiffness k was changed to different values during the simulation. The damping ratio ζ of the ground is set to 0.9. The corresponding damping coefficient c is calculated using the equation:

$$\zeta = \frac{c}{c_c} \tag{3.1}$$

with

$$c_c = 2\sqrt{km} \tag{3.2}$$

where m is the weight of the android and k is ground stiffness.

3.4 Reference Kinematic Data

Kinematic data of intact human walking on the solid surface was collected using motion capture cameras by Emiliano Jos Quiones Yumbla. The subject walked on the ASU Variable Stiffness Treadmill (VST) (Skidmore *et al.* (2015)) at a constant speed.

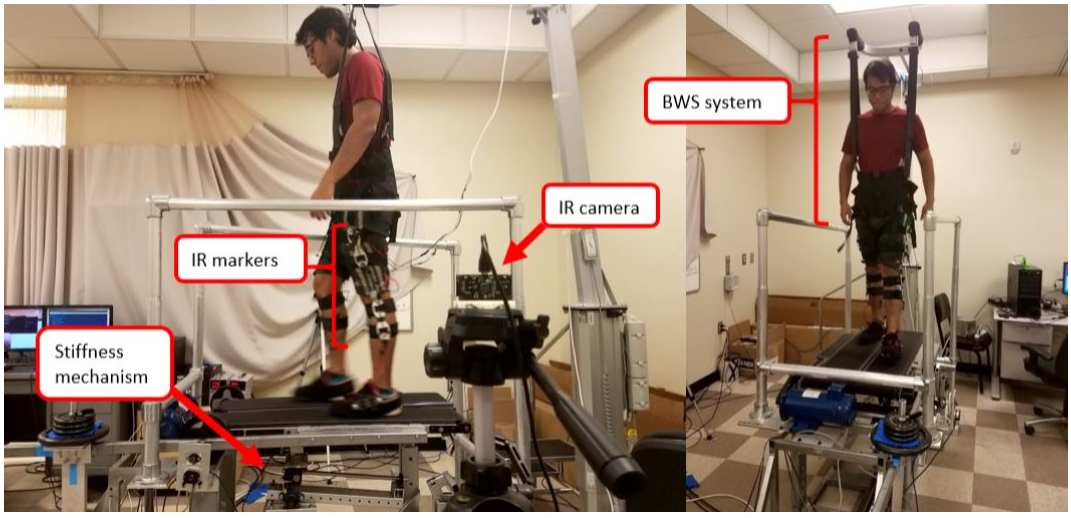

Figure 3.3: Subject Walking on the ASU VST, Fou (2018)

Twelve infrared LED markers (Super Bright LEDs Inc, model: IR-1WS-850) were placed at thigh, shank, and foot. Two infrared cameras (Code Laboratories Inc, model: DUO MINI LX) were placed on either side of the subject. After the calibration, the information of the markers relative positions compared to the initial condition is given by these cameras in real time and then saved in a .txt file. The data in this file is later extracted and converted into the angle profile of each joint using MATLAB. The mean of each joint angle profile is used as the reference kinematics data for the android to walk. These are illustrated below (Fig. 3.4, 3.5, 3.6).

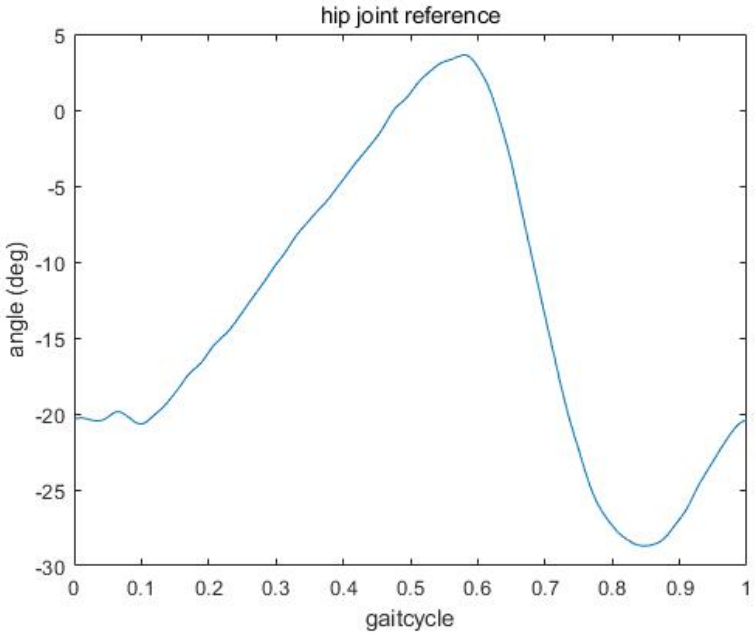

Figure 3.4: Hip Joint Reference Kinematics (Positive for Hip Extension)

3.5 PID Controller

In order to make the android able to walk, we need to create a closed-loop control for the joints. There are two choices in Simscape. The first one uses joint angle as input and the torque would be automatically computed while the second one uses torque as input and joint angle would be computed. Considering all the motors we

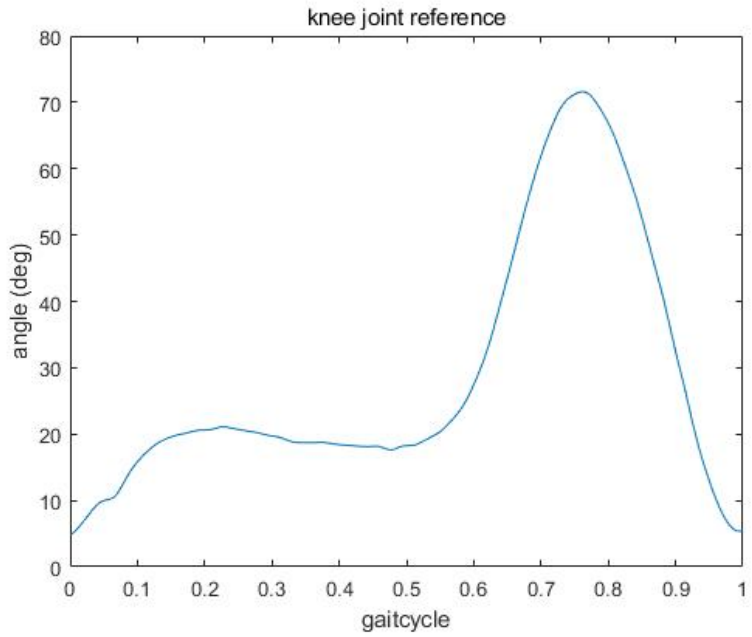

Figure 3.5: Knee Joint Reference Kinematics (Positive for Knee Flexion)

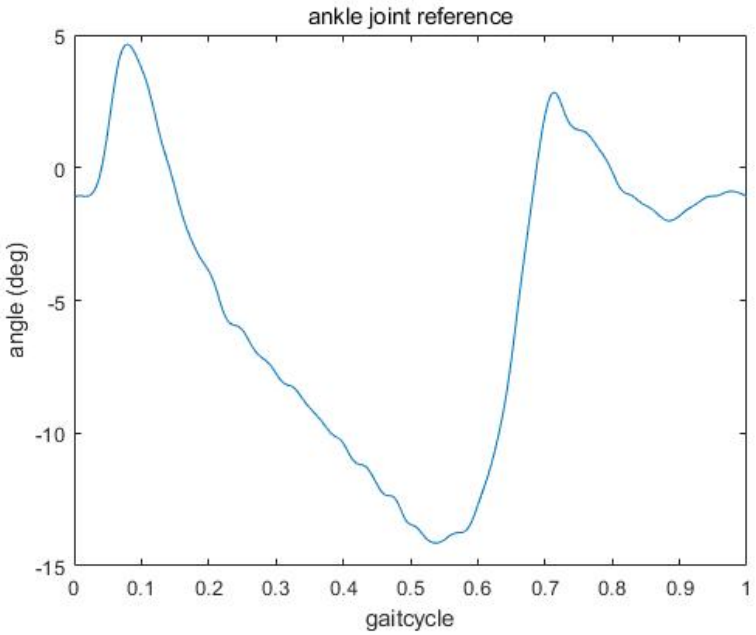

Figure 3.6: Ankle Joint Reference Kinematics (Positive for Ankle Plantar Flexion)

use in prosthesis output torque, the torque control mode was chosen.

PID controllers are widely used in control systems. It is one of the most important concepts in control history. Usually, a typical PID controller consists of a proportional

part (P), an integral part (I) and a derivative part (D). That is why it is called a PID controller.

Usually, the PID controller takes the error of current state and reference state as input. The proportional part gives feedback of the current error. The output of this part would be the gain Kp times error. With proportional control only, the system would not be able to compensate for the steady state error. Thus, we need an integral part to help to eliminate the remaining error. It is said that integral control is a measurement of the past error. The output of this part is the gain Ki times the sum of the past error. The bigger the error is, the faster the system can approach the desired value. That is, the integral part can accelerate the system response and eliminate steady-state errors. However, the integral part can also cause problems such as overshooting. Therefore, we need a new part to make up for the error caused by the integral part. Here comes the derivative part, which is considered to be a prediction of the future error. The output of this part is the gain Kd times the derivative of the system error. The derivative part can improve the stability of the system. While applying derivative control, a low pass filter is also added to it to restrict the effect of high frequency and noise. In the simulation, the following PID controller form is used:

$$P + I\frac{1}{s} + D\frac{N}{1 + N\frac{1}{s}} \tag{3.3}$$

where P is the proportional gain, I is the integral gain, D is the derivative gain and N is the filter coefficient. An example control block diagram used for each joint is shown in Fig. 3.7.

The difference between the current joint angle and the reference data is calculated and sent to the PID controller as an input. The PID controller gives torque as output which then drives the joint to move and changes its angle. A closed-loop control is

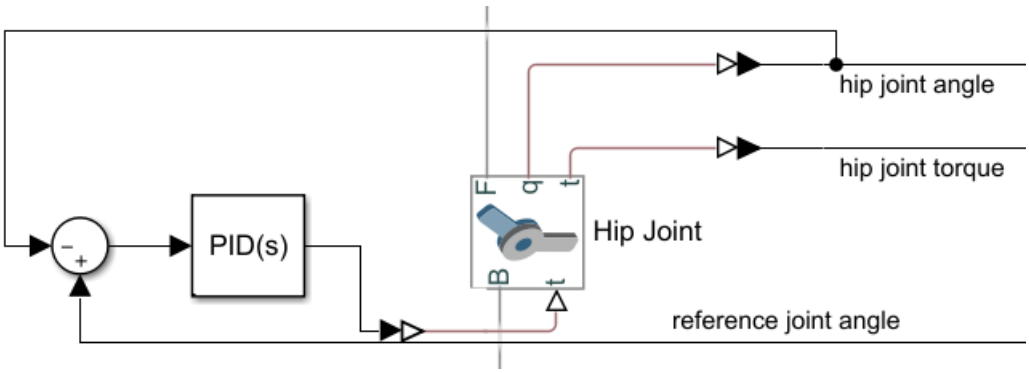

Figure 3.7: Example Control Block for Hip Joint

thereby created. Because the physical load is not the same for the 6 joints, three different PID controllers were designed separately for each joint. They were tuned manually and the gains are shown at the Table below.

Table 3.2: PID Controller Coefficients

Joint	**P**	**I**	**D**	**N**
Hip	6000	50	50	1500
Knee	12000	100	100	1500
Ankle	4600	20	60	1500

During the simulation, the controllers showed good performance. The actual joint angles were tracking the reference data well, as shown in Fig. 3.8. Although the performance varies while changing the ground stiffness, the differences are not large. For large stiffness cases, the performance is almost the same. However, for low stiffness cases such as 1,000 N/m, the PID controllers have a better performance with larger Kp and Kd in hip joint and larger Kp in ankle joint.

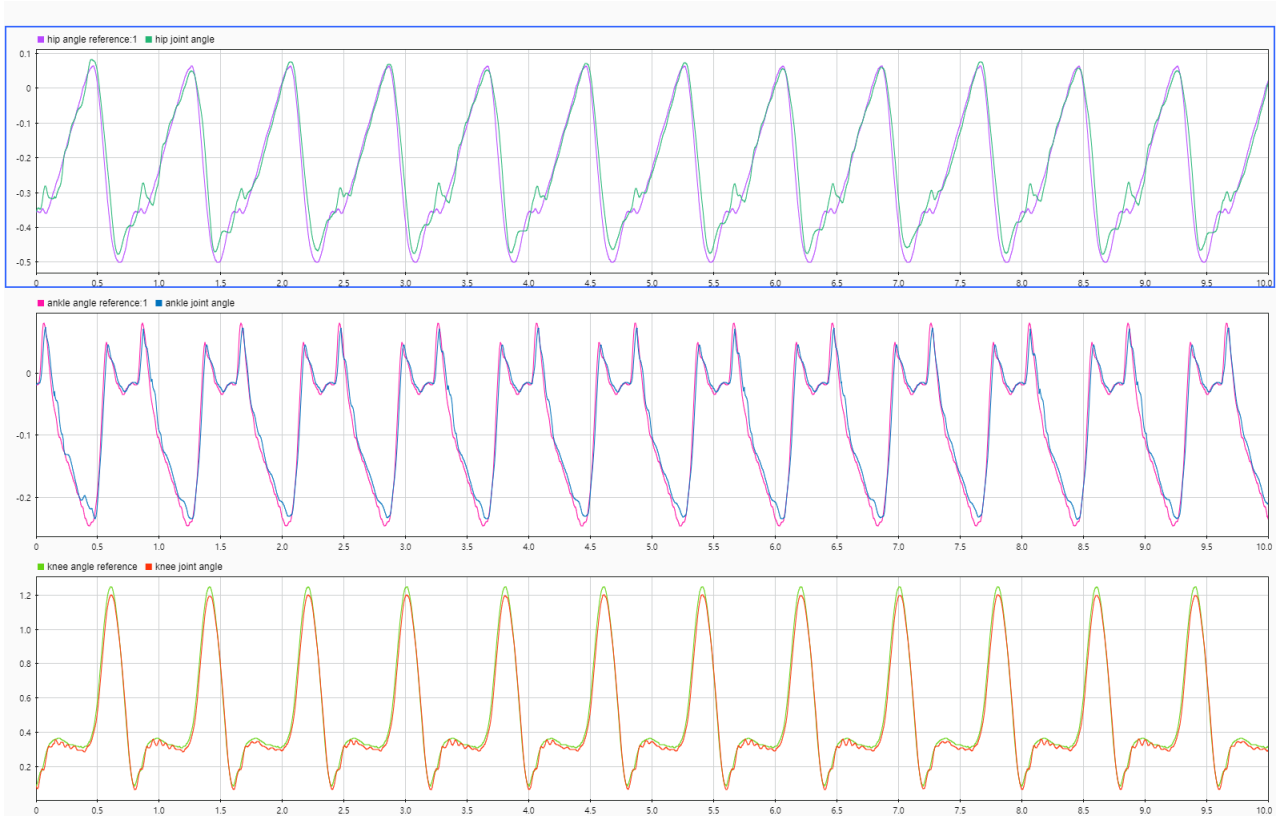

Figure 3.8: Actual Joint Angle Compared to Reference Joint Angle

Chapter 4

RESULTS AND DISCUSSION

In the simulation, the gait cycle is set to 0.8s long (75 strides per minute) and one trial has 12.5 gait cycles (10s). Multiple trials with different values of ground stiffness were done. The main purpose of this study is to see how the torque profile of each joint for the android to maintain the designated joint angle profile changes when walking on surfaces of different stiffness. Figure 4.1 showed an example of a full gait cycle starting from left leg heel strike and ending at left leg heel strike. The gait cycle has been equally divided into ten parts. The time interval between consecutive snapshots in Fig. 4.1 is 0.08s. The ground stiffness is set to 10000 N/m in this case.

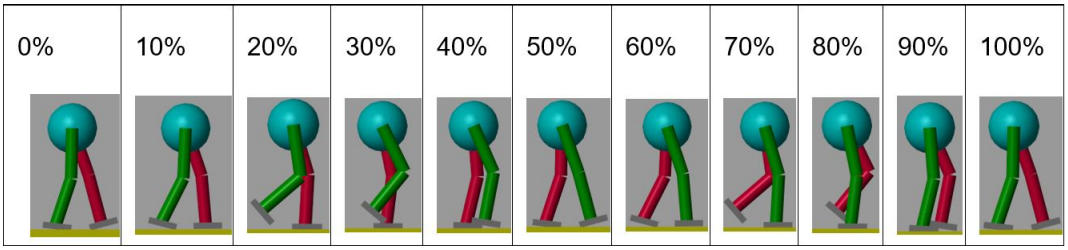

Figure 4.1: Full Gait Cycle

From the snapshots above, it can be seen that the android walked very similar to a human. This is because it was able to track the reference data well. A gait cycle can be divided into the stance phase and the swing phase. The stance phase starts with heel strike of one leg and ends with toe off of the same leg. In the plot shown above, the stance phase is approximately from 0% gait cycle to 60% gait cycle for left leg (the red one).

The android is walking forward only because of the contact between its feet and the ground, no other horizontal force is applied to this android. Thus, the android is

considered to be walking by itself, by only tracking the reference kinematic data by the PID controllers on the leg joints.

All data and plots presented in the following sections are collected from the androids left leg unless noted otherwise.

A typical set of hip torque profile acquired from the simulation is shown in Fig. 4.2. The ground stiffness, in this case, is 10,000 N/m.

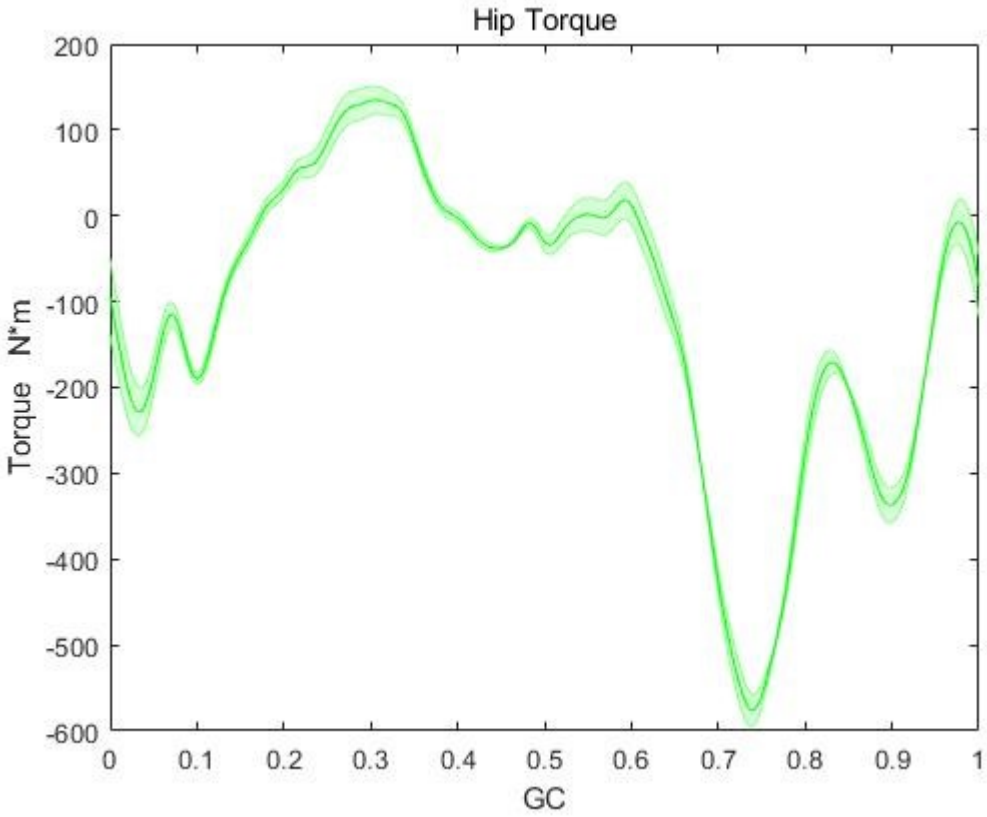

Figure 4.2: Hip Torque Profile in One Gait Cycle

For the hip torque profile, it is positive from about 20% to 40% GC and 50% to 60 % GC, which means the hip joint torque is trying to push the leg backward (hip extension). Taking the android movement into consideration, the android is standing on its left leg alone from 20% to 40% GC and is trying to move its right leg forward. This is reasonable as left leg is the only support the android can get rotate its right

part forward. From 50% to 60% GC, heel strike happens on its right leg. It is the so-called double support phase where the android stands on both legs. The hip extension happens here might be in order to produce the push-off force for the android to walk.

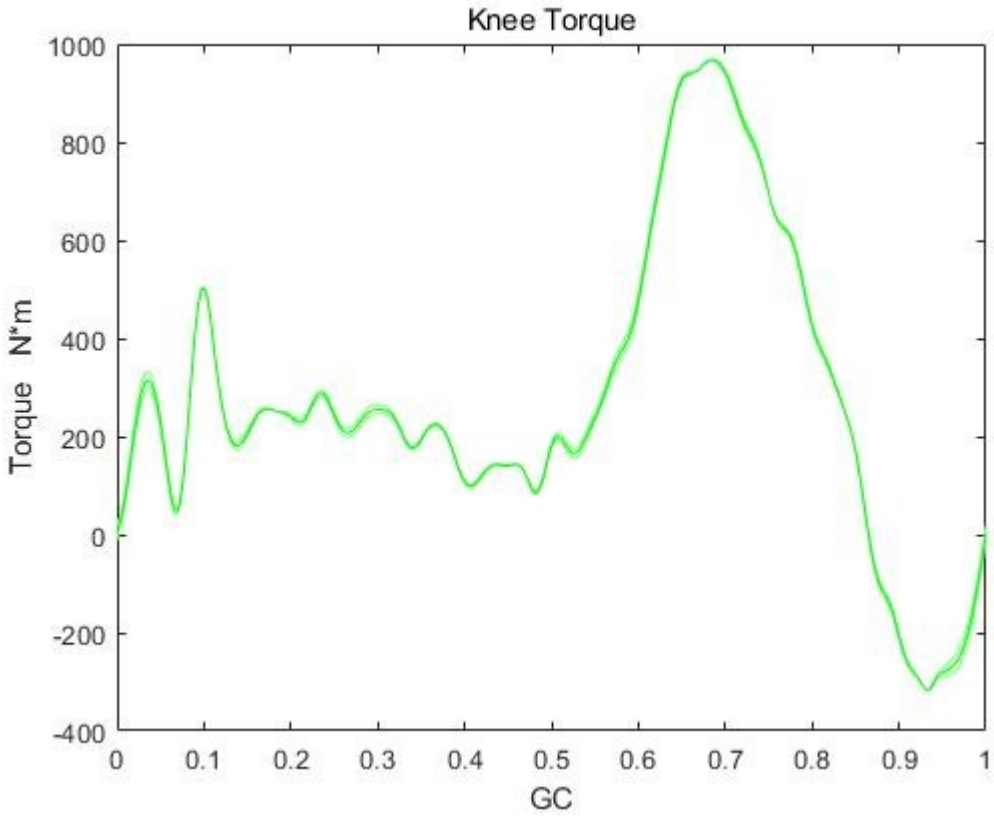

Figure 4.3: Knee Torque Profile in One Gait Cycle

For the knee torque profile shown in Fig. 4.3, it appears to be positive most of the time. It only goes to negative from approximately 85% to 100% GC. Recall that positive in knee joint means knee flexion. The knee joint is trying to bend during the whole stance phase and the early half of the swing phase. Recall the knee joint reference data, 70% to 100% GC is where it is decreasing meaning that the knee is experiencing extension. It seems to be reasonable that the torque is negative.

For the ankle torque profile shown in Fig. 4.4, contrary to knee torque profile, the negative values dominate. From 3.7% to 10.4%, 61.2% to 73.4% and 91.5% to

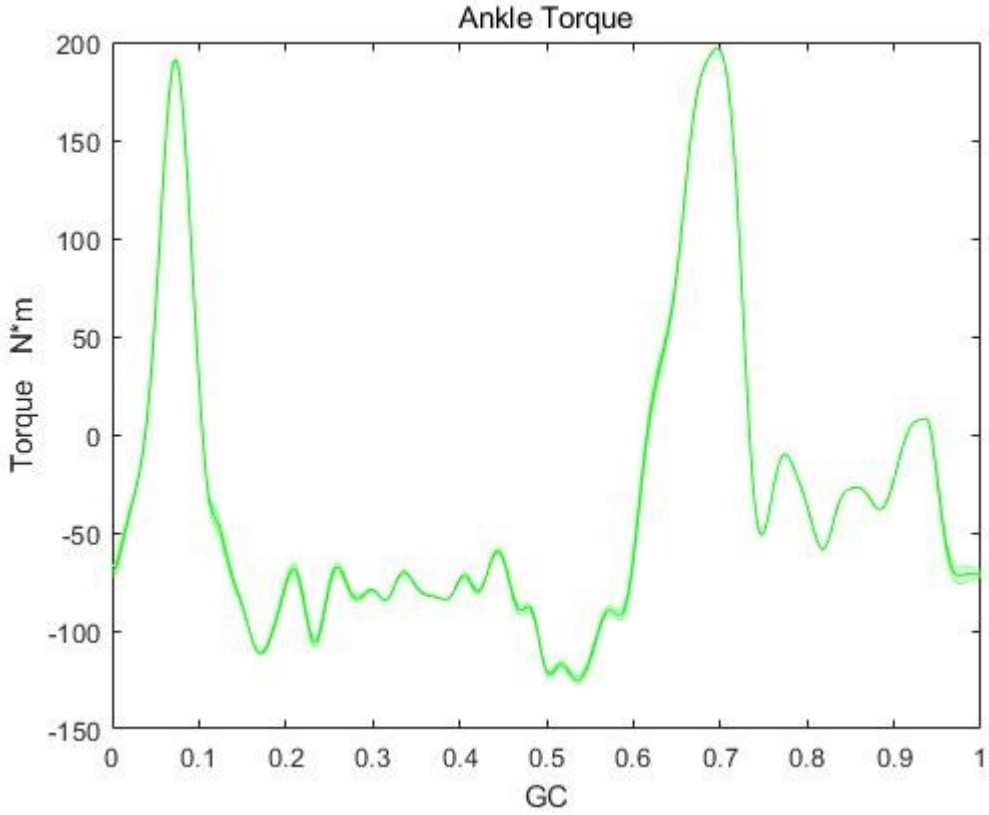

Figure 4.4: Ankle Torque Profile in One Gait Cycle

94.5% GC, the ankle joint is positive, pushing the foot backward (plantar flexion). The corresponding event is the initial contact and loading response, toe off and initial swing and terminal swing. Two peaks of ankle torque appear at 7% and 70% GC. A possible explanation is that during these periods, the ankle joint angle is increasing fastest which requires a large positive torque.

4.1 Stiffness Range: 10,000 N/m to 100,000 N/m

Although the joint torque profile is important, in this research, we are interested in the change of the torque profile when varying the ground stiffness. In order to get an overall look of it, ten simulations were done. The ground stiffness ranged from 10,000 N/m to 100,000N/m with an increment of 10,000N/m.

In Fig. 4.5, there are 3-D mesh plots for the torque profile (left column) and the difference between each simulation and the reference data (right column) of each joint. The torque profile when ground stiffness equals to 100,000 N/m was chosen to be the reference data. Notice that the same color does not represent the same value in different plots.

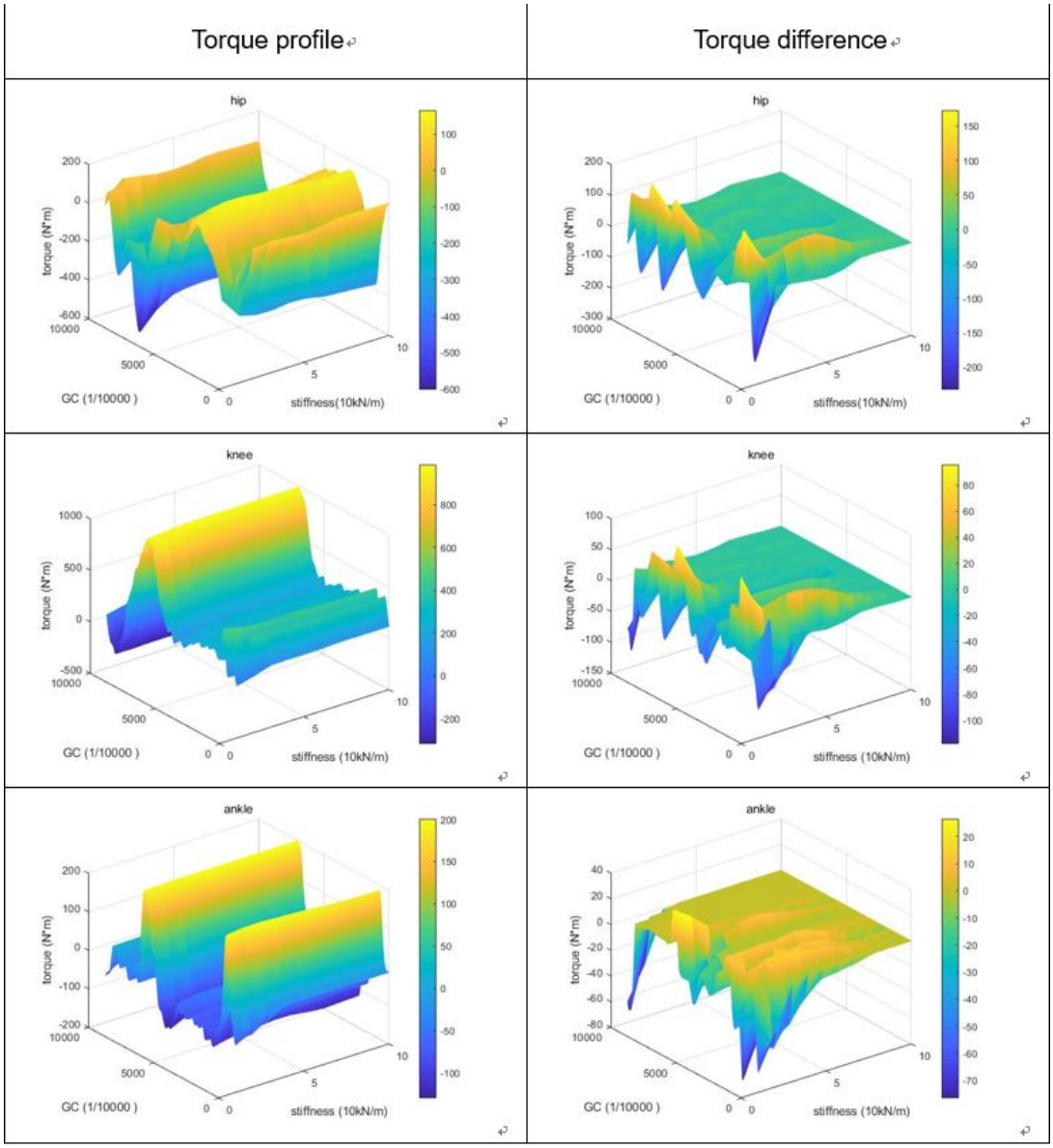

Figure 4.5: 3D Plot of Torque Profile and Its Change When Ground Stiffness Was Increased from 10,000 N/m to 100,000 N/m

From the left column, it can be seen that as ground stiffness increases, the torque profile almost remains the same in shape. The peak positions (yellow and blue) seem to be in the same position. In the right column where the difference between the torque profile of each simulation and the reference data are plotted, two interesting observations can be made. The first one is that the torque difference tends to be diminished to zero as ground stiffness increases. That is to say, for sufficiently large ground stiffness, the torque profile appears to be unchanged. However, in the low stiffness part, the differences are quite obvious. The second observation is that the change of torque profile in the first half gait cycle seems to be larger than in the latter half. This might be because of the contact between the leg and ground happens from 0% to 60% GC. This direct contact brings a larger effect to this leg.

4.2 Stiffness Range: 1,000 N/m to 30,000 N/m

As discussed in the previous section, the torque profile tends to be unaffected by the change in ground stiffness if the stiffness is sufficiently large. Thus, the focus was put on the low stiffness range (1,000 N/m to 30,000 N/m). 30 simulations were done in this range, in which the stiffness was increased from 1,000 N/m to 30,000 N/m by 1,000 N/m each time.

Like in the previous section, torque profile and torque difference are also plotted in 3D-mesh. The plots are arranged in Fig. 4.6. The torque profile of the case where ground stiffness is 30,000 N/m was chosen as the reference data.

It appears that there is a critical point at ground stiffness around 10,000 N/m. For cases with ground stiffness smaller than this value, the torque profile changes rapidly and irregularly. However, for those with stiffness larger than this value, there seem to be smoother trends in the change of torque profile.

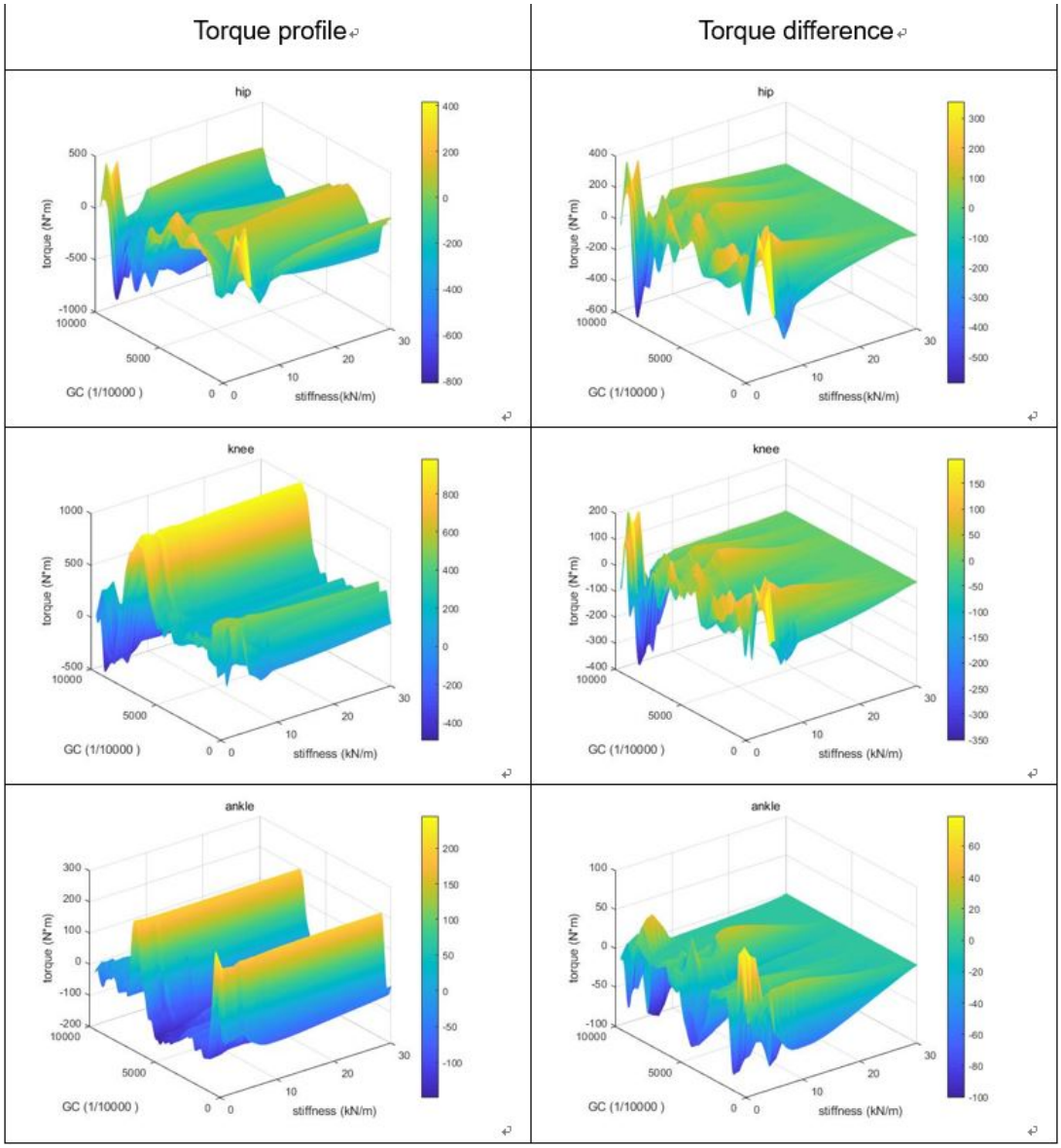

Figure 4.6: 3D Plot of Torque Profile and Its Change When Ground Stiffness Was Increased from 1,000 N/m to 30,000 N/m

4.2.1 Stiffness Range: 10,000 N/m to 30,000 N/m

The 3D mesh can give an overall view of how the torque profile changes when varying stiffness, but it hardly gives any detailed information. In order to see what exactly happened when the ground stiffness increased from 10,000 N/m to 30,000 N/m, 2D plots are employed. Torque profiles of 5 different cases were put together to compare (see Fig. 4.7).

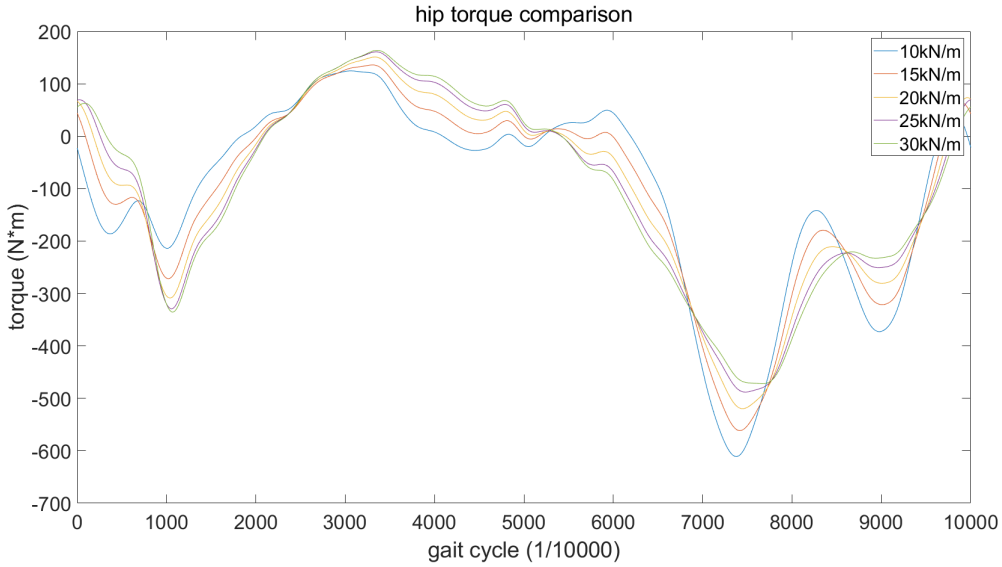

Figure 4.7: Hip Joint Torque Comparison for Stiffness of 10kN/m, 15kN/m, 20kN/m, 25kN/m and 30kN/m

For hip torque, it first increases during 0% to about 7% GC and then decreases until 25% GC. From 25% GC to 53%, the torque grows larger as stiffness increases. However, after 53% GC and up to 67% GC, it goes down again. During 77% GC to 85% GC and 95% to 100% GC, the trend is to decrease. For the else of GC, it is an increase. These percent GCs are not precise values for the change to happen. Although the lines seem to intersect at some point, for example, 67% GC, their intersection is actually moving slightly as stiffness increases. Recall that toe off happens around 60% GC. There are some interesting observations when taking that into account. Notice

that the torque profile of 10,000N/m has two peaks from 15%GC to 65% GC while in the 30,000 N/m case, there is only one obvious peak. The second peak appears at 60% GC tends to shrink as stiffness increases and the first peak keeps growing. That is to say, the hip torque increases in the middle of the stance phase and decreases at toe off. The second observation is that hip torque tends to increase at heel strike and decreases at the start of single leg support (around 10% GC). The last observation is, that during the swing phase, the torque profile is becoming smoother as stiffness increases. From 67% GC to 95% GC, all the peaks are becoming smaller no matter they are positive or negative.

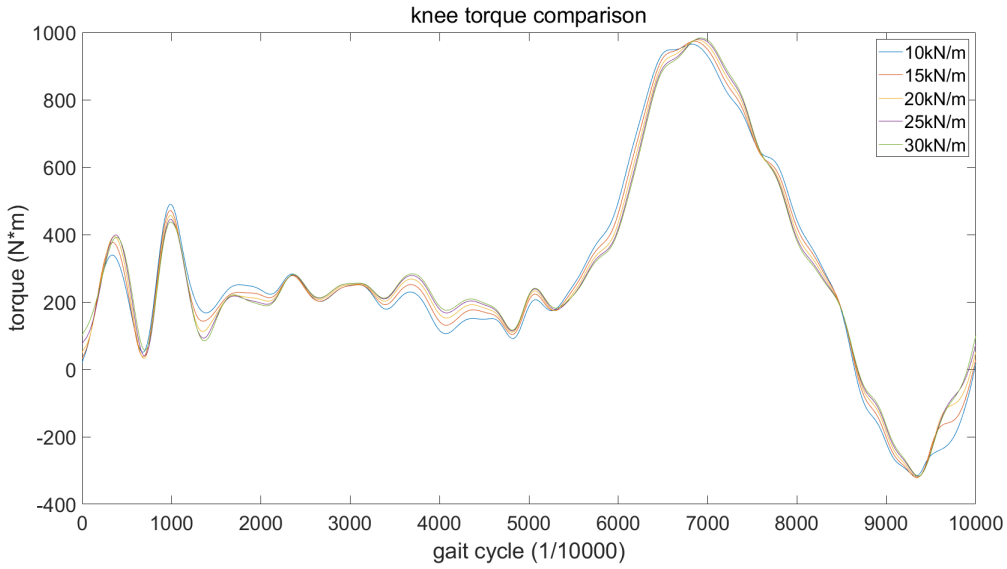

Figure 4.8: Knee Joint Torque Comparison for Stiffness of 10kN/m, 15kN/m, 20kN/m, 25kN/m and 30kN/m

For the knee joint (see Fig. 4.8), similar trends as the hip joint are detected. However, the deviations of the torque profile across different stiffnesses are smaller than the hip joint. The torque seems to increase during 0% to 6%, 23% to 53%, 67% to 75% and 85% to 100% GC while decreasing for most of the rest period of the gait cycle. Relating the changes of torque profile to the events happened in the gait cycle, it is noticeable that at the start of single leg support and around heel strike, the

knee joint torque decreased. For the decrease happened around 80% GC, no certain event can be found from the animation. But if we take the knee joint angle profile into consideration, that is where the joint angle peak is. Although there are many differences in the torque profile, the most obvious deviations occur in three places which are 15% GC (the beginning of single leg support), 40% GC (mid to terminal stance) and 97% GC (terminal swing to heel strike).

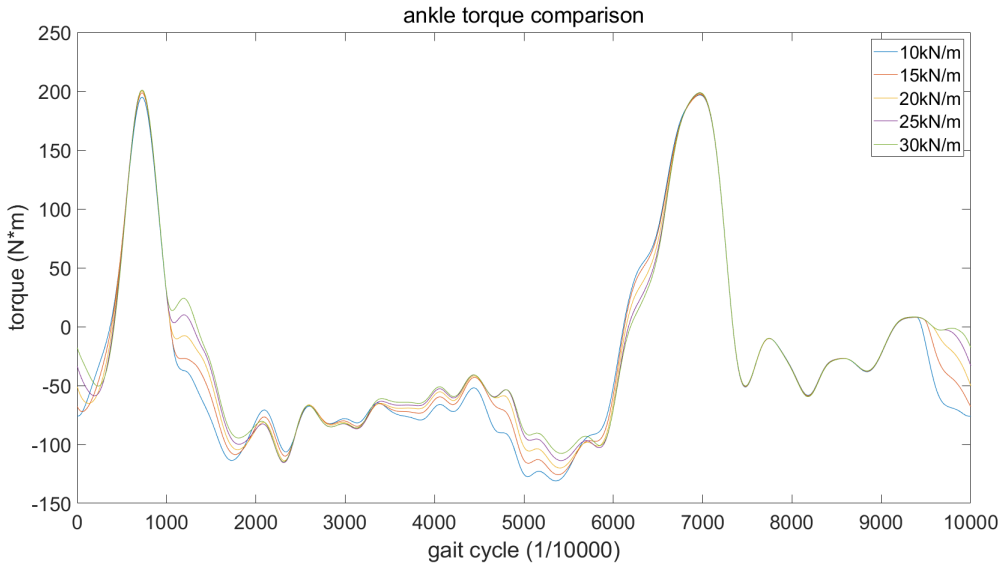

Figure 4.9: Ankle Joint Torque Comparison for Stiffness of 10kN/m, 15kN/m, 20kN/m, 25kN/m and 30kN/m

For ankle joint (see Fig. 4.9), an increase in torque profile as stiffness increases can be observed during the most time of the gait cycle. Especially for 10% to 20%, 34% to 57% and 94% to 100% which corresponds to start of single leg support, mid to terminal stance and terminal swing. At around 60% GC which is supposed to be toe-off, the torque decreases as stiffness increases. During most of the swing phase, there is almost no change in torque with respect to stiffness. This is quite reasonable since the foot is lifted in the air and has no contact with the ground.

4.2.2 Stiffness Range: 1,000 N/m to 10,000 N/m

The torque profiles show good trends for ground stiffness ranging from 10,000N/m to 30,000 N/m. But recall the 3D plot, the low stiffness range seems to be more rapidly changing. One possible explanation could be that, in cases of low stiffness such as 1,000 N/m, the android showed obvious signs of sinking into the ground. The vertical displacement is quite large, almost ten times the value compared to large-stiffness cases. The android moved up and down as if it was floating in the water when walking on the surface with extremely low stiffness.

4.3 Limitations and Future Work

The proposed model has the following limitations.

The first limitation is that although this model looks like a 3D one, the dynamics are still computed in a 2D way. As it has no arms and an actual upper body, it is hard for it to balance on the frontal plane in the 3D environment. In order to improve this, a well-designed upper body should be included in the future version. Also, the experimental data of upper body movement and arm swing should be recorded and imported into this model.

The second limitation is that the feet of this model are rigid bodies. However, actual human feet are elastic and flexible. This has caused one problem that was observed during the simulation which is the foot could stick on the ground upon heel strike or toe off. Since the android was not aware that it was stuck and kept following the reference joint angle profile, it might bounce on the ground. The contact force between the bouncing foot and the ground will be smaller and it might just slide on the ground. In order to solve this, one possible solution is to add an additional toe joint to the foot to make the foot length variable.

The third limitation comes from the reference data. As mentioned before, the data was collected from an intact subject walking on a solid surface. This requires the android to have the same physical parameters as the subject has, for example, thigh length and shank length. It is noticeable that with the same joint angle profile, different leg length would give different results. Just imagine one android with zero thigh length and one with zero shank length, the results would be totally different. Also, the parameter difference might cause the same problem as the second limitation, the bouncing robot. To solve this problem, a simple way is to collect the subject's biological data at the same time. A possible alternate solution would be the same as proposed for solving the second limitation, that is to make the foot flexible.

The fourth limitation is the joint model. All the joint in the simulation has the same parameters all the time. However, the actual impedance of the human joint would change with respect to muscle activation. For example, the ankle stiffness is said to be larger during the stance phase (Lee *et al.* (2016)). Future improvements may require taking these into consideration. It would be great if a model of the relationship between joint impedance and muscle activities can be built.

Chapter 5

CONCLUSIONS

From the simulation results, there are differences in torque profile while walking on compliant surfaces. Since torque is actually a vector, by taking direction into account, some conclusions can be made.

For the hip joint, increase in value happens at heel strike, single leg support, initial swing, and terminal swing. Meaning that, at heel strike, toe off and some period in swing phase, the torque tends to decrease in one direction, and then turns to the opposite direction as stiffness increases.

For the knee joint, the magnitude of torque vector decreases at the start of single leg support, toe off, initial swing, and terminal swing.

For the ankle joint, the decrease of the magnitude of torque vector happens at heel strike, the start of single leg support, contralateral leg heel strike, toe off and terminal swing.

The purpose of this research is to help the design of ankle prosthesis for compliant surface walking. One possible application of the results presented above could be changing the output of the motor upon certain event being detected. As mentioned before, the IMU on the ankle prosthesis that is currently being used, could provide the information of the movement of the shank and thus determine what period it is in a full gait cycle. The EMG sensors can give feedback of muscle activation which appears to be different when walking on compliant surfaces; the above could result in useful information about the ground stiffness. Then, according to the stiffness predicted, the motor on the ankle prosthesis can be commanded to provide more torque at heel strike, toe- off and so on, based on the ground compliance.

REFERENCES

Albert, A. and W. Gerth, "Analytic path planning algorithms for bipedal robots without a trunk", Journal of Intelligent and Robotic Systems **36**, 2, 109–127 (2003).

Au, S., M. Berniker and H. Herr, "Powered ankle-foot prosthesis to assist level-ground and stair-descent gaits", Neural Networks **21**, 4, 654–666 (2008).

Au, S. K., H. Herr, J. Weber and E. C. Martinez-Villalpando, "Powered ankle-foot prosthesis for the improvement of amputee ambulation", in "2007 29th annual international conference of the IEEE engineering in medicine and biology society", pp. 3020–3026 (IEEE, 2007).

Borzova, E. and Y. Hurmuzlu, "Passively walking five-link robot", Automatica **40**, 4, 621–629 (2004).

Chow, C. and D. Jacobson, "Studies of human locomotion via optimal programming", Mathematical Biosciences **10**, 3-4, 239–306 (1971).

Collins, S., A. Ruina, R. Tedrake and M. Wisse, "Efficient bipedal robots based on passive-dynamic walkers", Science **307**, 5712, 1082–1085 (2005).

Fou, L., *Indicators of Anticipated Walking Surface Transitions for Powered Prosthetic Control*, Ph.D. thesis, Arizona State University (2018).

Grimmer, M., M. Holgate, R. Holgate, A. Boehler, J. Ward, K. Hollander, T. Sugar and A. Seyfarth, "A powered prosthetic ankle joint for walking and running", Biomedical engineering online **15**, 3, 141 (2016).

Huang, Q., K. Yokoi, S. Kajita, K. Kaneko, H. Arai, N. Koyachi and K. Tanie, "Planning walking patterns for a biped robot", IEEE Transactions on robotics and automation **17**, 3, 280–289 (2001).

Kajita, S., O. Matsumoto and M. Saigo, "Real-time 3d walking pattern generation for a biped robot with telescopic legs", in "Proceedings 2001 ICRA. IEEE International Conference on Robotics and Automation (Cat. No. 01CH37164)", vol. 3, pp. 2299–2306 (IEEE, 2001).

Kajita, S. and K. Tani, "Study of dynamic biped locomotion on rugged terrain-derivation and application of the linear inverted pendulum mode", in "Proceedings. 1991 IEEE International Conference on Robotics and Automation", pp. 1405–1411 (IEEE, 1991).

Larsen, W. J., *Anatomy: development, function, clinical correlations* (Saunders Philadelphia, 2002).

Lee, H., E. J. Rouse and H. I. Krebs, "Summary of human ankle mechanical impedance during walking", IEEE journal of translational engineering in health and medicine **4**, 1–7 (2016).

Li, C., M. Tokuda, J. Furusho, K. Koyanagi, S. Morimoto, Y. Hashimoto, A. Nakagawa and Y. Akazawa, "Research and development of the intelligently-controlled prosthetic ankle joint", in "2006 International Conference on Mechatronics and Automation", pp. 1114–1119 (IEEE, 2006).

McGeer, T. *et al.*, "Passive dynamic walking", I. J. Robotic Res. **9**, 2, 62–82 (1990).

Miller, S. and T. MathWorks, "Modeling physical systems as physical networks with the simscape language", in "6th Vienna International Conference on Mathematical Modelling (MATHMOD 2009), Vienna, Austria, February", pp. 11–13 (2009).

Miller, W. C., M. Speechley and B. Deathe, "The prevalence and risk factors of falling and fear of falling among lower extremity amputees", Archives of physical medicine and rehabilitation **82**, 8, 1031–1037 (2001).

Nolan, L., A. Wit, K. Dudziñski, A. Lees, M. Lake and M. Wychowañski, "Adjustments in gait symmetry with walking speed in trans-femoral and trans-tibial amputees", Gait & posture **17**, 2, 142–151 (2003).

Park, J. H. and K. D. Kim, "Biped robot walking using gravity-compensated inverted pendulum mode and computed torque control", in "Proceedings. 1998 IEEE International Conference on Robotics and Automation (Cat. No. 98CH36146)", vol. 4, pp. 3528–3533 (IEEE, 1998).

Perry, J., J. R. Davids *et al.*, "Gait analysis: normal and pathological function", Journal of Pediatric Orthopaedics **12**, 6, 815 (1992).

Schmalz, T., S. Blumentritt and R. Jarasch, "Energy expenditure and biomechanical characteristics of lower limb amputee gait:: The influence of prosthetic alignment and different prosthetic components", Gait & posture **16**, 3, 255–263 (2002).

Simscape, T., "Users guide, the mathworks", (2018).

Skidmore, J., A. Barkan and P. Artemiadis, "Variable stiffness treadmill (vst): System development, characterization, and preliminary experiments", IEEE/ASME Transactions on Mechatronics **20**, 4, 1717–1724 (2015).

Vukobratović, M. and B. Borovac, "Zero-moment pointthirty five years of its life", International journal of humanoid robotics **1**, 01, 157–173 (2004).

Vukobratovic, M. and D. Juricic, "Contribution to the synthesis of biped gait", IEEE Transactions on Biomedical Engineering , 1, 1–6 (1969).

Xiang, Y., J. S. Arora and K. Abdel-Malek, "Physics-based modeling and simulation of human walking: a review of optimization-based and other approaches", Structural and Multidisciplinary Optimization **42**, 1, 1–23 (2010).

Ziegler-Graham, K., E. J. MacKenzie, P. L. Ephraim, T. G. Travison and R. Brookmeyer, "Estimating the prevalence of limb loss in the united states: 2005 to 2050", Archives of physical medicine and rehabilitation **89**, 3, 422–429 (2008).